Research Square

Preprints are preliminary reports that have not undergone peer review.
They should not be considered conclusive, used to inform clinical practice,
or referenced by the media as validated information.

Urban morphology, not scale, dominates building-operational carbon emissions across 520 million buildings in China

Dabo Guan

guandabo@tsinghua.edu.cn

Department of Earth System Sciences, Tsinghua University https://orcid.org/0000-0003-3773-3403

Yuxing Chen

Tsinghua University

Kaipeng Ren

College of Science, China University of Petroleum(Beijing)

Yida Sun

Department of Earth System Science, Ministry of Education Key Laboratory for Earth System Modeling, Institute for Global Change Studies, Tsinghua University https://orcid.org/0000-0001-8160-1358

Quan Wen

Department of Earth System Science, Tsinghua University

Diling Liang

The Bartlett School of Sustainable Construction, University College London, London, UK

Yuli Shan

University of Birmingham https://orcid.org/0000-0002-5215-8657

Article

Keywords:

Posted Date: November 27th, 2025

DOI: https://doi.org/10.21203/rs.3.rs-8093398/v1

License: This work is licensed under a Creative Commons Attribution 4.0 International License.
Read Full License

Additional Declarations: There is **NO** Competing Interest.

Urban morphology, not scale, dominates building-operational carbon emissions across 520 million buildings in China

Yuxin Chen[1], Kaipeng Ren[2], Yida Sun[1], Diling Liang[3], Quan Wen[1], Yuli Shan[4], Dabo Guan[1,3 *]

Affiliations:

1. Department of Earth System Science, Tsinghua University, Beijing 100084, China.
2. College of Science, China University of Petroleum (Beijing), Beijing 102249, China.
3. The Bartlett School of Sustainable Construction, University College London, London WC1E 7HB, UK.
4. School of Geography, Earth and Environmental Sciences, University of Birmingham, Birmingham B15 2TT, UK

Abstract

Building are responsible for 37% of global energy-related CO_2 emissions, yet the operational carbon of building stocks is still predominantly assessed at aggregated statistical scales or for small, non-representative samples. This obscures how the physical configuration of cities shapes their emission profiles. **Here**, we construct a spatially explicit, bottom-up inventory of building operational carbon emissions(BOCE) for China that couples city-level energy statistics with morphological and functional data for more than 520 million individual buildings across 330 prefecture and 2,633 counties. In 2021, Chinese buildings emitted 2,767 Mt CO_2, with pronounced spatial clustering that aligns with major urban agglomerations but exhibits far stronger variation in carbon intensity than in total emissions. We show that urban form—not city size or economic scale—is the primary determinant of BOCE intensity. A systematic morphological paradox emerges: districts with low building density but high floor area ratio host vertically concentrated high-rise clusters dispersed over large areas and become carbon hotspots, frequently exceeding 15 kg CO_2 m^{-2}—a level higher than that observed in 71% of all districts—whereas compact, morphologically coherent developments sustain much lower intensities. Case studies of five representative cities spanning distinct climates and urban forms reveal a nearly three-fold range in intensity (10.27–28.82 kg CO_2 m^{-2}) despite comparable total emissions, arising from interactions among climate, building typology and energy infrastructure. Our multi-scale framework demonstrates that redesigning spatial configuration and power systems can decouple urban development from emissions, providing actionable pathways for context-specific decarbonization in rapidly urbanizing regions.

1. Introduction

Climate change represents one of the most pressing “grey rhinos” confronting humanity in this decade[1]. However, the timely and effective implementation of climate policies remains insufficient in most countries[2,3]. As the next round of Nationally Determined Contributions (NDCs) under the

Paris Agreement—targeting emission reductions by 2035—is expected to be released by 2025[4], China faces only 35 years to achieve its carbon neutrality goal[5]. Recently, China announced its 2035 NDC to strengthen climate action, aiming to reduce economy-wide net greenhouse gas emissions by 7–10% from their peak levels[6]. Although cities occupy less than 2% of the Earth's surface, they account for over 75% of global energy consumption and approximately 70% of CO_2 emissions[7,8], underscoring their central role in decarbonization efforts. Building operations alone account for about 30% of global final energy use[9] and contribute 26% of global energy-related CO_2 emissions[10], including 22% of China's total energy-related CO_2 emissions[11]. These facts highlight the critical importance of assessing city-level BOCE to support China's long-term carbon neutrality ambitions.

The building sector has long been recognized as the final frontier for decarbonization[12]. Accurate accounting of building operational energy consumption and BOCE forms the foundation for achieving life-cycle carbon neutrality in buildings[13], as BOCE contributes approximately 70–90% of total life-cycle building emissions[14]. Although BOCE has been widely studied, existing research often suffers from scale limitations—being either too broad, encompassing city[15], provincial[16], national[17,18] or regional[19,20] levels to capture technological heterogeneity, or too narrow, focusing on individual[21] or small groups of buildings[22], which constrains the generalization of emission patterns. China is currently undergoing large-scale urban renewal under its national territorial spatial planning framework, presenting a critical window for emission mitigation. Targeted strategies could reduce residential building emissions by up to 43% between 2023 and 2060[23]. The forthcoming government-led urban renewal initiative, set to commence in 2025, is expected to play a pivotal role by accelerating the renovation of aging residential communities and promoting energy-efficient retrofits[23]. Güneralp et al.(2017) further emphasized that developing countries can substantially reduce building cooling and heating demands by adopting higher urban density modes[24]. As urban renewal inherently alters building density—and consequently affects BOCE—developing a detailed typological characterization of buildings becomes essential. Such characterization enables high-resolution BOCE assessments by integrating spatial information, offering critical insights for reducing building energy consumption and associated emissions[25].

An expanding body of research has sought to integrate building typology into frameworks for accounting BOCE[26,27]. Building density—commonly defined as a two-dimensional metric—effectively captures intra-urban built form and differentiates morphological patterns[28], such as compact urban cores versus peripheral zones, thereby revealing spatial inequalities[29]. Recent studies further emphasize the importance of three-dimensional indicators in characterizing urban morphology, with the floor area ratio (FAR) emerging as the most widely adopted metric[30]. The impact of FAR on building energy performance, however, varies substantially across climate zones[31,32], highlighting significant spatial heterogeneity across large territories such as China. Despite its relevance, most analyses linking FAR and energy use remain confined to a few buildings or meso-scale case studies[33] within single cities, limiting their generalizability to broader geographic contexts. From the perspectives of research scalability and policy relevance, a BOCE accounting framework that incorporates multi-tiered data (e.g., provincial, municipal, district, and street levels) and multi-dimensional attributes—spanning building types and individual structural characteristics[22]—is crucial for deepening our understanding of how urban form and architectural configuration shape energy demand[34,35]. Yap et al.(2025) demonstrate that while urban and building

densities are strongly correlated, high-density development is not a one-size-fits-all solution due to complex emission dynamics mediated by local climatic, technological, and socio-economic contexts[36]. Yet their analysis, constrained by data availability, covers only five global cities. This underscores the prevailing limitation of high-resolution studies, which typically focus on representative cities within specific climate zones and fail to capture the heterogeneity observed at broader provincial or national scales. China's recent BOCE dataset—covering 321 cities from 2015 to 2020 through a combination of "top-down" and "bottom-up" methods[37]—marks a significant advancement in spatially explicit emissions accounting. However, the absence of detailed building typology information at the community level, primarily due to reliance on statistical rather than geospatial data, leaves a critical research gap. Bridging this gap requires constructing high-resolution, large-scale BOCE datasets to unravel the complex interplay between building morphology and emissions. Moreover, existing studies have largely overlooked rural areas[38] and small- to medium-sized cities[24 39], thereby limiting the formulation of inclusive decarbonization strategies beyond major metropolitan regions..

Data-driven and physics-based simulation methods are widely employed to examine the relationship between building typology and BOCE. Among simulation tools, EnergyPlus (E+)[40] stands out as a benchmark physical model, serving as the computational backbone for other urban-scale energy simulation platforms such as CityBES[41], UMI[42] and SimStadt[43]. Since its release by the U.S. Department of Energy, E+ has garnered considerable attention within the research community. In parallel, Chinese researchers have developed DeST, a simulation model integrated with CAD software that enables micro-scale energy simulations of individual buildings from a designer's perspective[44]. However, physics-based simulation models require highly detailed input parameters—most of which remain unavailable at citywide or national scales[45]. Data-driven approaches have therefore emerged as a promising alternative, extracting morphological and spatial features from open-source datasets such as remote sensing imagery and Geographic Information Systems (GIS)[46]. While these "bottom-up" approaches perform well in assessing the energy consumption and CO_2 emissions of individual buildings, they operate primarily at the micro scale and struggle to generate results that are directly comparable with macro-level statistical data encompassing cities, provinces, or nations. Conversely, "top-down" approaches—such as those based on the Kaya identity—offer a robust means of capturing aggregate patterns in national[47] and provincial[16] energy consumption and CO_2 emissions. Yet, they lack the capacity to reveal morphological or typological characteristics of the built environment. Although numerous studies from developed economies[48]—particularly within the European Union[35,49], where data quality and standardization are high—have examined the energy implications of building typology at national scales, their focus on major urban centers in advanced economies[36] has led to an underrepresentation of emerging nations. The persistent scarcity of high-resolution data and in-depth analyses for developing cities[50] continues to impede the design of effective, evidence-based decarbonization strategies at the global scale[51].

In this study, we develop a bottom-up, spatially explicit emissions inventory encompassing 330 prefecture-level cities and 2,633 county-level administrative units, covering more than 520 million individual buildings. On the demand side, detailed physical and functional attributes—such as geographical location, footprint, total floor area, number of stories, and building use type—are

incorporated to accurately estimate operational energy consumption. On the supply side, we couple this building-level demand with a dataset of 30,745 point-source power generation units, accounting for each unit's fuel type, technological configuration, operational lifespan, dispatch regime, and generation efficiency. This integrated framework enables high-resolution estimation of both Scope 1 and Scope 2 emissions with enhanced spatial precision and reliability, producing a robust multi-scale dataset that captures urban–rural disparities and systemic emission patterns (see Methods 4.1 for details). Importantly, the study boundary extends beyond major metropolitan areas to include medium- and small-sized cities as well as rural regions, thereby addressing the persistent research gap in these underrepresented areas. Based on this dataset, a set of indicators is developed to characterize the multi-dimensional features of cities' BOCE. Specifically, building density and floor area ratio (FAR) are employed to represent two- and three-dimensional spatial characteristics, while building area and height describe individual structural attributes. Together, these indicators reveal the spatial heterogeneity of China's urban BOCE through the lens of building typology. Considering socio-economic conditions and urban morphology, five representative cities from distinct climate zones and morphological categories are selected for detailed case studies: Shenzhen (compact city), Yangzhou (traditional dense city), Guiyang (mountain-cluster city), Lanzhou (linear valley city), and Daqing (resource-based dispersed city). Through this classification, our study seeks to unravel the interplay among BOCE, building intensity, FAR, climate zone, and micro-level characteristics—such as building type, height, and area—thereby providing a scientific foundation for formulating refined and spatially differentiated urban decarbonization policies.

2. Results

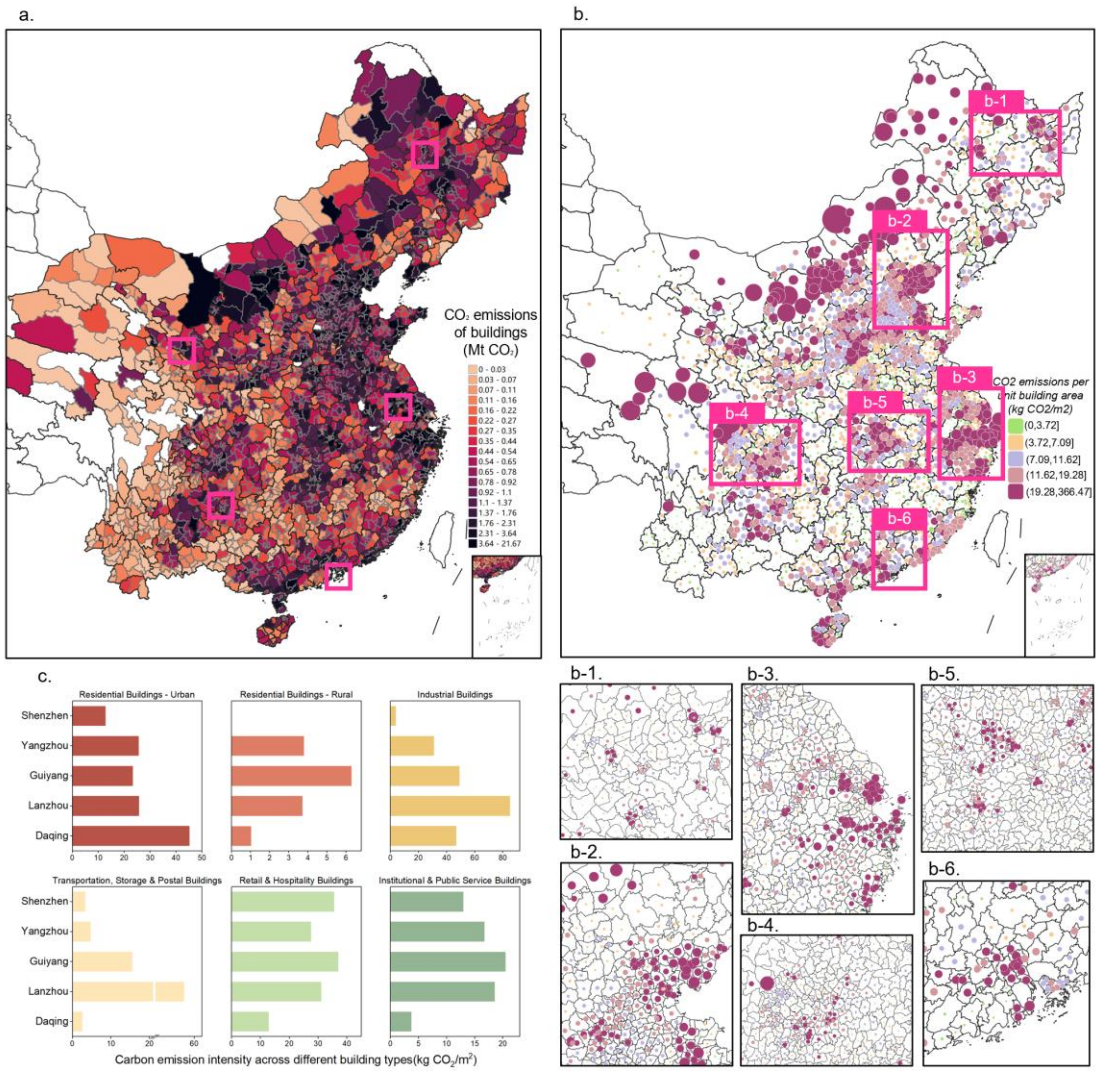


Fig.1 | Spatial distribution of building operational CO_2 emissions across Chinese administrative units (2021). a illustrates the spatial heterogeneity of building operational carbon emissions (Scope 1 + Scope 2) across China's 330 prefecture-level cities and 2,633 county-level administrative units, with color gradients indicating emission magnitude from low (light tones) to high (dark tones). **b** quantifies emission intensity (**kg CO_2 m^{-2}**) at county level, using quintile classification (five equal-frequency categories) with chromatic variations denoting intensity ranges and circle diameters representing within-category variance. Panels **b-1** to **b-6** present magnified views of the six major urban agglomerations in a: Harbin-Changsha (**b-1**), Beijing-Tianjin-Hebei (**b-2**), Yangtze River Delta (**b-3**), Chengdu-Chongqing (**b-4**), Middle Yangtze River (**b-5**), and Pearl River Delta (**b-6**), highlighting spatial patterns of emission intensity within each urban cluster. Panel **c** depicts the carbon emission intensity per unit floor area, disaggregated by building type, for five representative cities (Shenzhen, Yangzhou, Guiyang, Lanzhou, and Daqing) located across distinct climate zones in China. The methodology for building classification is detailed in Supplementary Table 1.

In 2021, the total operational carbon emissions from building energy use across Chinese cities reached approximately 2,767 Mt CO_2. This vast total, however, displays a distinctly clustered spatial

pattern that aligns closely with China's six major urban. These regions—characterized by strong economic output, integrated industrial systems, and dense populations—exhibit both high emission magnitudes and pronounced spatial concentration. Among them, the Yangtze River Delta stands out as the largest emitter, accounting for 441.71 Mt CO_2, largely driven by key cities such as Shanghai (68.54 Mt), Hangzhou (59.30 Mt), and Suzhou (43.64 Mt). As China's primary hub for logistics, trade, and finance, this region also sustains the nation's largest population base. The Beijing–Tianjin–Hebei agglomeration follows, contributing 373.00 Mt CO_2 in the same year. Notably, the Harbin–Changchun urban cluster also records substantial emissions, reflecting both its status as the principal economic center in Northeast China and its harsh cold climate. Extended winter heating demands under cold and arid conditions further intensify its carbon footprint.

Figure **1b** illustrates the carbon emissions per unit floor area—hereafter referred to as carbon intensity—showing that regions with high building carbon intensity are predominantly concentrated in northern China, north of the Qinling–Huaihe Line, with the exception of several economically developed clusters in the south. The ten administrative districts with the highest carbon intensity are mainly distributed across Heilongjiang, Inner Mongolia, and Qinghai, all exceeding 120 kg CO_2 m^{-2}. In contrast, the lowest-intensity districts are largely located in Guangxi Zhuang Autonomous Region and Yunnan Province. Remarkably, 86% of districts in Guangxi and over 90% in Yunnan exhibit below-average carbon intensity, owing to their mild year-round climate and cleaner energy mix. A comparative analysis of total operational carbon emissions and carbon intensity across districts reveals a generally positive correlation. Among all administrative units, 524 districts display both high total emissions and high intensity, while 1,537 districts exhibit low values for both, together accounting for 78.3% of the total. Interestingly, 332 districts show low total emissions but high intensity, with Inner Mongolia alone contributing 10% of these cases. This paradox arises from Inner Mongolia's vast land area and sparse population, where small building scales—combined with low-density development, carbon-intensive energy structures, and inefficient technologies—result in high emission intensity despite relatively low absolute emissions. Conversely, 234 districts exhibit the opposite pattern: high total emissions but low intensity, predominantly in Shandong Province. This reflects Shandong's extensive building stock and large total floor area, which, despite substantial overall emissions, yield comparatively favorable intensity levels.

The calculated operational carbon intensities across five representative Chinese cities—Shenzhen, Yangzhou, Guiyang, Lanzhou, and Daqing—reveal distinct emission profiles (Fig. 1c) shaped by variations in economic structure, climatic conditions, and infrastructural development. In the industrial sector, carbon intensity spans a wide range, from 3.85 kg CO_2 m^{-2} in Shenzhen—reflecting its transition toward a high-tech, service-oriented economy—to 85.02 kg CO_2 m^{-2} in Lanzhou and 49.12 kg CO_2 m^{-2} in Guiyang, consistent with their roles as a traditional heavy-industrial base and an emerging data-center hub, respectively. Both cities depend heavily on energy-intensive industries with relatively low energy efficiency. Yangzhou exhibits a moderate level (30.97 kg CO_2 m^{-2}), aligning with its lighter manufacturing profile. A clear north–south gradient emerges in the urban residential sector, driven primarily by heating demand. Northern cities such as Daqing (45.08 kg CO_2 m^{-2}) and Lanzhou (25.68 kg CO_2 m^{-2}) record the highest intensities due to widespread coal-based centralized heating, whereas transitional cities like Yangzhou (25.57 kg CO_2 m^{-2}) and Guiyang (23.26 kg CO_2 m^{-2}) show moderate values. The lowest intensity occurs in Shenzhen (12.76

kg CO_2 m^{-2}), where energy use is dominated by cooling and appliances. Notably, Daqing's exceptionally low rural carbon intensity (1.01 kg CO_2 m^{-2}) likely reflects a statistical artifact—stemming from low occupancy rates or unrecorded energy use—rather than genuinely high efficiency.

Beyond the industrial and residential sectors, variations in the transportation and hospitality domains further emphasize the functional and structural heterogeneity of urban emissions. Lanzhou's notably high carbon intensity in transportation and postal facilities (57.40 kg CO_2 m^{-2}) likely reflects its role as a major logistics hub in Northwest China, compounded by the relatively low energy efficiency of its supporting infrastructure. In contrast, the elevated intensities observed in the retail and hospitality sectors of Shenzhen (35.55 kg CO_2 m^{-2}) and Guiyang (37.00 kg CO_2 m^{-2}) indicate robust commercial activity and thriving tourism, whereas Daqing's markedly lower value (12.85 kg CO_2 m^{-2}) points to limited service demand. Collectively, these patterns underscore a key insight: urban carbon footprints are inherently heterogeneous across functional categories and are shaped by a city's developmental stage, industrial composition, geographic setting, and energy infrastructure. Such multidimensional characterization is crucial for designing targeted, context-specific decarbonization pathways at the city scale.

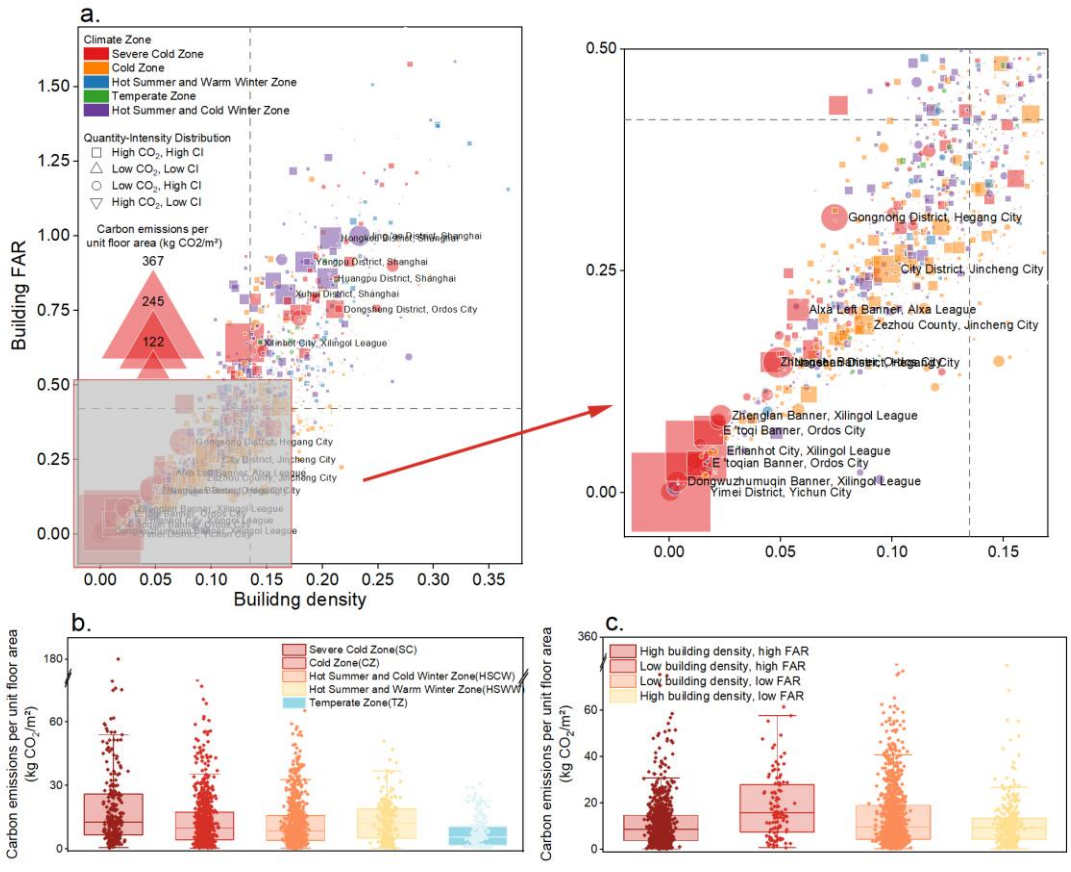


Fig.2 | Carbon intensity and its heterogeneous drivers across Chinese administrative districts. This figure illustrates county-level variations in building operational carbon intensity. **a**, Relationship between carbon emissions per unit floor area (kg CO_2 m^{-2}) and two key structural indicators—building density (x-axis) and floor area ratio (y-axis). The vertical and horizontal dashed lines denote their respective mean values, dividing the scatter plot into four quadrants. Point colors represent climate zones, sizes indicate emission intensity, and shapes correspond to four characteristic combinations of total emissions and intensity: high–high, low–low, low–high, and high–low. An inset panel provides an enlarged view for clarity. **b** stratifies emission intensity by five climate zone classifications, while **c** categorizes intensity according to four building characteristic combinations.

The majority of administrative districts cluster in Quadrants I and III of Fig. 2a, reflecting the inherent positive correlation between building density and floor area ratio. Notably, Quadrant I predominantly contains districts from hot summer/cold winter and hot summer/warm winter climate zones, while Quadrant III is heavily populated by cold and severe cold climate regions. Quantitative analysis reveals a marked disparity in carbon intensity, with Quadrant I districts averaging 11.67 kg CO_2 m^{-2} compared to 15.36 kg CO_2 m^{-2} in Quadrant III. These findings align with established literature demonstrating that higher urban density and floor area ratio correlate with reduced building carbon emissions and intensity, thereby validating our preliminary observations.

Analysis of Fig. 2b shows that among all climate zones, administrative districts in severe-cold regions exhibit both the highest mean carbon emissions per unit building area and the largest variance in emission values. The magnified view in Fig. 2a further highlights Yimei District—the political, economic, and cultural center of Yichun City in Heilongjiang Province, China's northernmost region—as having the most extreme carbon intensity, reaching 366.47 kg CO_2 m^{-2}. This exceptionally high value arises from three interrelated factors. First, Yichun's harsh climate demands over six months of annual heating, making thermal energy the dominant emission source. Second, the district's building stock characteristics amplify emission intensity: despite increasing residential vacancy rates driven by outmigration, the centralized heating system continues to operate at full spatial and temporal coverage. Third, extensive heating infrastructure supporting Yimei's administrative functions, coupled with a low-density urban expansion pattern, results in long pipeline networks and significant thermal distribution losses. Notably, among the five climate zones classified in this study, temperate regions exhibit the lowest mean carbon intensity, averaging only 7.71 kg CO_2 m^{-2}—underscoring the profound influence of climatic conditions on building-related emissions.

Building upon the climate zone analysis, administrative districts were further classified into four urban morphological typologies—high-density–high-FAR, low-density–high-FAR, low-density–low-FAR, and high-density–low-FAR—as illustrated in Fig. 2c Comparative assessment of carbon intensity across these categories reveals that districts characterized by low building density yet high FAR exhibit the highest mean carbon intensity, averaging 15.36 kg CO_2 m^{-2}. Notably, four of the ten most carbon-intensive districts in this group are located in Shanghai—Songjiang (57.78), Jiading (55.43), Minhang (49.39), and Qingpu (40.09 kg CO_2 m^{-2})—with two others in Hangzhou, including

Binjiang District (41.59 kg CO_2 m^{-2}). The elevated carbon intensity in these low-density–high-FAR configurations arises from the interplay of architectural form and climatic context. Vertically concentrated high-rise structures combined with horizontally dispersed urban layouts lead to operational inefficiencies, primarily by amplifying wind pressure differentials that heighten ventilation loads and diminish HVAC performance. Moreover, the Yangtze River Delta's hot-summer/cold-winter climate imposes dual seasonal energy demands, further intensified by the low-density urban form. In winter, reduced windbreak effects from sparse building arrangements elevate heating requirements, while in summer, inadequate shading and increased solar gain drive cooling loads. These compounding effects render low-density–high-FAR developments particularly carbon-intensive, underscoring the complex interdependence between urban morphology and climatic conditions in shaping building operational emissions.

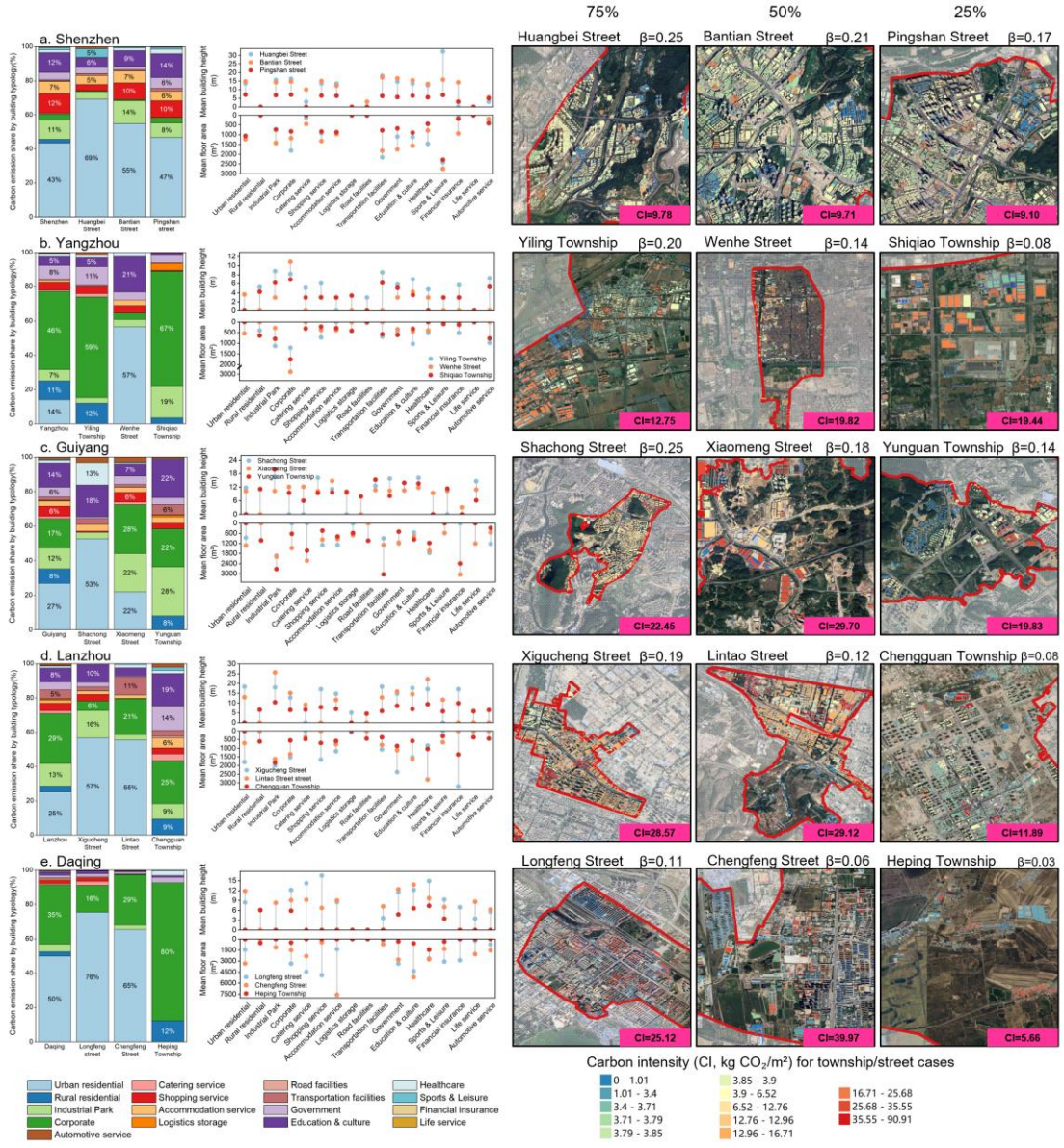


Fig.3 | Mechanistic analysis of urban carbon intensity variations based on individual building characteristics. The figure presents a comparative analysis across five representative cities: Shenzhen (**a**), Yangzhou (**b**), Guiyang (**c**), Lanzhou (**d**), and Daqing (**e**). For each city, township or street-level samples at the 75th, 50th, and 25th percentiles of building density are examined. Stacked bar charts show the composition of emissions by building type for both the citywide average and the selected township or street cases. Companion lollipop plots display the average building height and footprint area for these samples. Topographic maps on the right visualize building-specific carbon intensity (CI, kg CO_2 m^{-2}) for the same cases, with β values indicating local building density. Red outlines delineate administrative boundaries of the featured streets; areas beyond these boundaries, which lie outside the analytical scope, are masked in grey for visual clarity. All panels are shown at consistent scales to enable cross-city comparison of emission patterns. The base map was created in QGIS (v. 3.28.11-Firenze; https://www.qgis.org) using data from the Standard Map Service of the Ministry of Natural Resources of China (Review Map No.: GS(2019)1822; http://bzdt.ch.mnr.gov.cn/). Copyright of the base geographic data belongs to the Ministry of Natural Resources. The satellite imagery basemap is derived from the ESRI World Imagery service (accessible via the XYZ Tiles function in QGIS), which provides global multisource imagery primarily from commercial and public datasets including Landsat and Sentinel.

Our analysis identifies five archetypal Chinese cities—Shenzhen, Yangzhou, Guiyang, Lanzhou, and Daqing—each situated in a distinct climatic zone and characterized by unique urban morphological parameters such as building density and FAR. These cities embody fundamentally different models of urban development: Shenzhen exemplifies compact vertical urbanization; Yangzhou preserves traditional morphology with moderate-density, low-rise configurations; Guiyang represents topographically constrained, clustered development; Lanzhou exhibits a linear river-valley form; and Daqing typifies resource-based cities with expansive, low-density layouts. Despite comparable aggregate building operational emissions across the five cities (12–15 Mt CO_2 annually), their carbon intensity metrics reveal pronounced spatial heterogeneity, ranging from 10.27 kg CO_2 m^{-2} in Shenzhen's energy-efficient high-rises to 28.82 kg CO_2 m^{-2} in Lanzhou's energy-intensive valley developments, with Yangzhou (15.38), Guiyang (21.65), and Daqing (17.58 kg CO_2 m^{-2}) exhibiting intermediate values. This sharp divergence in emission efficiency—despite similar total outputs—underscores the pivotal influence of urban form and regional climate in shaping building energy metabolism and highlights the necessity of tailoring decarbonization strategies to distinct urban morphologies.

Climatic conditions are fundamental determinants of operational carbon emissions in buildings, with thermal demand variations across climate zones directly shaping energy consumption patterns. Shenzhen, located in a subtropical monsoon climate with persistently high temperatures, experiences dominant cooling demand in summer and negligible heating in winter, resulting in relatively low carbon intensity. In contrast, Lanzhou (temperate continental climate) and Daqing (cold temperate climate) endure long, severe winters that necessitate carbon-intensive centralized heating systems—particularly Lanzhou's coal-fired cogeneration—producing substantially higher emission intensities. Yangzhou and Guiyang occupy intermediate climatic zones, yet Guiyang's humid plateau environment, combined with insufficient building insulation, amplifies winter

heating demand, explaining its higher carbon intensity relative to Yangzhou. These findings are consistent with prior research indicating that heating accounts for 40–60% of total building energy consumption in cold regions, whereas cooling dominates in warmer climates. Notably, Daqing's seemingly moderate citywide carbon intensity conceals substantial intra-urban disparities: urban districts connected to centralized heating systems reach nearly 30 kg CO_2 m^{-2}, while rural areas (Heping Township)—reliant on unrecorded traditional heating methods such as kang stoves, coal furnaces, or biomass due to dispersed settlements and high infrastructure costs—remain largely excluded from both heating networks and official energy statistics. This discrepancy highlights how aggregate urban-scale indicators can obscure critical spatial emission patterns, underscoring the need for multi-scale and high-resolution carbon accounting to reveal localized dynamics.

The composition of building types directly shapes energy consumption patterns, producing pronounced variations in carbon intensity across cities. In Shenzhen, building-related emissions are dominated by the residential (45.52%) and commercial (19.31%) sectors. The latter's centralized air-conditioning systems and stricter energy efficiency standards contribute to relatively low energy use per unit area. By contrast, Yangzhou and Lanzhou exhibit substantially higher shares of industrial buildings (52.34% and 42.23%, respectively), where the energy intensity of heavy industrial and ancillary facilities significantly elevates overall carbon emission intensity. These findings are consistent with the China Building Energy Efficiency Report (CABEE, 2021)[52], which indicates that industrial buildings consume two to three times more energy per unit area than residential buildings. Guiyang presents a more balanced emission structure, yet concentrated energy use in scientific, educational, and medical buildings (15.63%)—driven by high-power laboratory and hospital equipment—exerts upward pressure on its aggregate carbon intensity.

The vertical dimension and spatial configuration of buildings indirectly shape carbon emission intensity by influencing three critical factors: building envelope thermal performance, energy system efficiency, and local microclimatic conditions. As illustrated by the lollipop charts in Fig. 3a, Shenzhen's predominance of high-rise buildings confers dual advantages. Centralized energy systems, such as district air-conditioning, generally operate with higher efficiency than decentralized alternatives, while dense urban form reduces winter heat loss through shared building envelopes. In contrast, Yangzhou's low-rise building stock (3–12 m) exhibits poor thermal insulation and limited centralized energy management, resulting in elevated energy consumption per unit area. Topographical constraints in valley cities such as Lanzhou often necessitate higher floor area ratios to offset land scarcity, giving rise to distinctive linear urban forms. Although Lanzhou includes some energy-efficient mid- and high-rise residential buildings (6–25 m), their potential benefits are offset by spatial dispersion that increases energy distribution losses and by suboptimal insulation standards that undermine the advantages of vertical development. Daqing, a resource-dependent city, features low-rise, ultra-low-density, and spatially dispersed building patterns, where large inter-building distances complicate energy management and lead to disproportionately high carbon emissions per unit floor area. Collectively, these findings demonstrate that while vertical urban development can enhance energy efficiency through intensive resource utilization, realizing its full low-carbon potential depends on the integration of high-performance building envelopes and centralized, high-efficiency energy systems.

3. Discussion

This study provides the first nationwide, high-resolution assessment of BOCE in China, the inclusion of 330 cities and 2,633 counties across China provides a comprehensive foundation for revealing how the spatial heterogeneity of emissions is deeply rooted in the interplay between urban morphology, building typologies, and climatic regimes. Our results demonstrate that emission intensity is not merely a function of energy consumption, but rather a systemic outcome of how cities grow, build, and adapt to environmental constraints. Northern cities—characterized by severe winters, coal-dependent energy systems, and low-density urban expansion—exhibit both high total emissions and elevated carbon intensity, underscoring the climatic and infrastructural barriers to decarbonization. Conversely, southern regions benefit from milder climates and cleaner power mixes, though some fast-growing clusters in the hot-summer/cold-winter zone show rising emissions due to inefficient building envelopes and decentralized air-conditioning. Under the growing frequency and severity of extreme weather events, including both harsh winter cold and intense summer heat[53 54,55], these areas are projected to experience sharp increases in energy demand and emissions from heating, ventilation, and air-conditioning (HVAC) systems. These contrasting patterns suggest that urban form and climatic stress jointly determine emission efficiency: compact, thermally efficient morphologies tend to decouple economic activity from carbon output, while dispersed layouts amplify heating and cooling demand.

The pronounced disparities In carbon emissions and Intensity across the five representative Chinese cities arise from the complex interactions among climatic conditions, urban morphology, building typology, and energy supply structures, highlighting the necessity of tailored mitigation strategies that integrate both demand- and supply-side dimensions. **On the supply side**, we further analyze the urban power systems of five representative cities (see Supplementary Fig. 3) to reveal critical insights into their decarbonization pathways from two complementary perspectives. cities exhibit pronounced differences in the carbon intensity of electricity, ranging from 0.159 kg CO_2 kWh^{-1} in Shenzhen to 0.974 kg CO_2 kWh^{-1} in Daqing—reflecting divergent generation portfolios and the uneven progress of energy transitions. Shenzhen's low-carbon profile stems from its reliance on nuclear and natural gas, illustrating the effectiveness of diversifying away from coal through stable, zero-carbon baseloads, whereas cities such as Lanzhou and Daqing remain constrained by coal dependency despite notable renewable expansions. Achieving deep decarbonization in these regions therefore requires not only scaling renewable capacity but also systematically retiring fossil-based assets and modernizing power grids to enable flexible, low-carbon dispatch. **On the demand side**, the spatial and structural characteristics of buildings strongly influence renewable energy utilization and operational efficiency. Medium- to low-density industrial cities such as Yangzhou and Daqing exhibit higher photovoltaic (PV) deployment potential due to abundant roof space (Scheme 2 in Supplementary Fig. 3f), while dense, high-rise cities like Shenzhen face spatial constraints that necessitate innovative solutions such as building-integrated photovoltaics (BIPV), façade-mounted systems, and integration with district cooling networks[56] to offset space-cooling emissions[57]. In contrast, mountainous and cloudy regions such as Guiyang must complement limited solar resources with energy-efficiency retrofits, improved building insulation, and alternative renewables such as small-scale hydropower or wind. For cities characterized by aging building stocks and coal-based

grids, as in Lanzhou, improving the performance of existing residential buildings and accelerating grid decarbonization are critical, while sprawling low-density cities such as Daqing would benefit from upgrading heating networks, utilizing industrial waste heat, and developing clustered renewable microgrids to reduce transmission losses. Collectively, these findings emphasize that aligning urban energy planning with local morphology, climate, and infrastructural conditions is essential to designing resilient, context-sensitive pathways for urban decarbonization.

In summary, this study highlights the necessity of developing context-specific urban carbon reduction strategies that account for the intricate interactions among built form, energy infrastructure, and local climate. The findings establish a structured framework for green urban planning that can be extended to cities with comparable morphological and climatic characteristics. A key limitation of this work is that it considers only operational carbon emissions from buildings. Incorporating embodied emissions across the full building life cycle—such as those associated with material production, transportation, and construction—would likely alter the emission profiles observed here. In particular, Shenzhen's emissions may increase substantially due to its high volume of new construction, whereas cities like Lanzhou and Daqing, characterized by predominantly older building stocks, would exhibit relatively smaller changes.

4. Methods

4.1 Calculation of Operational Carbon Emissions from Buildings

4.1.1 Top-Down Approach for Estimating Operational Carbon Emissions

The top-down carbon accounting approach employed in this study is grounded in city-level energy balance tables from the China Emission Accounts and Datasets (CEADs; https://www.ceads.net.cn/) [58,59], through which energy consumption across various sectors is allocated to different building types. For cities lacking such data, a downscaling procedure was applied to estimate city-level energy use from provincial energy statistics. This approach follows the sectoral downscaling framework proposed by Shan et al. (2019)[60], utilizing representative socioeconomic indicators to distribute provincial energy data to the city level. The method ensures a consistent and economically rational allocation of provincial statistics across cities, thereby enabling the disaggregation of energy consumption into distinct building categories even in the absence of direct city-level records. The resulting energy estimates were then incorporated into the top-down carbon accounting framework to calculate building operational emissions with enhanced spatial resolution and sectoral coherence.

For the household consumption sector, population was used as the scaling index. For the other sectors—including industry, transportation, services, and construction—the economic output values of corresponding sectors (i.e., gross output of secondary and tertiary industries) were employed as proxies. The city-to-province percentage p for each sector is defined as:

$$p = \frac{I_{city}}{I_{province}} \times 100\% \quad (1)$$

Where I_{city} and $I_{province}$ denote the scaling index of the city and the province, respectively. Using this ratio, the energy consumption of sector i in city c (EC_i^{city}) was derived from the energy consumption of the corresponding province p in the same sector ($EC_i^{province}$) as follows:

$$EC_i^{city} = EC_i^{province} \times p \quad (2)$$

As outlined above, this study focuses on energy consumption and the associated carbon emissions during the operational phase of buildings. From the consumption perspective, operational CO_2 emissions encompass both direct (Scope 1) and indirect (Scope 2) sources. Direct emissions arise from the on-site combustion of primary fuels—such as coal, oil, and natural gas—including natural gas and liquefied petroleum gas used for cooking, and coal used in decentralized heating. Indirect emissions, by contrast, stem from electricity consumption for lighting, appliances, and other electric-powered devices, as well as from heat used in centralized heating systems. Accordingly, this study accounts for five energy types: coal, oil, natural gas, electricity, and heat. Carbon emissions for each energy type are calculated based on their consumption volumes and corresponding emission factors.

For energy accounting, buildings are categorized into the following types for separate calculations: urban residential, rural residential, industrial buildings, transportation/warehouse/postal buildings, wholesale/retail/hotel/catering buildings, and science/education/culture/health/sports buildings. The sectoral disaggregation and matching methodology based on the energy balance table is described in the Table1.

Table 1 Sectoral Disaggregation and Matching Methodology Based on Energy Balance Table

NO.	Energy Balance Table Sector	Statistical Coverage	Building Energy Consumption	Included in This Study?	Building Type	Excluded Energy Types
①	Agriculture, Forestry, Animal Husbandry, and Fishery	Primary industry energy use	Does not include building energy use	No	—	—
②	Industry	Secondary industry energy use, including mining, manufacturing, and public utility production and supply	Includes building energy use (e.g., office buildings, staff dormitories)	Yes (excluding mining-related sectors)	Industrial buildings	Exclude kerosene, gasoline, diesel, and fuel oil
③	Construction	Secondary industry energy use related to construction activities	Similar to sector ②	No	—	—
④	Transportation, Warehousing, and Postal Services	Rail, road, waterway, air, pipeline, urban public transport, and related handling, storage, and postal services	Includes functional building energy use (e.g., stations, airports, post offices)	Yes (100% of coal consumption + 40% of electricity consumption)	Transportation/warehouse/postal buildings	Kerosene, gasoline, diesel, and fuel oil attributed to mobile emission sources
⑤	Wholesale, Retail, Hotel, and Catering Services	Tertiary industry dominated by service sectors	Primarily building energy use, but includes transportation energy within the sector	Yes	Wholesale/retail/hotel/catering buildings	
⑥	Others	Mainly covers other tertiary sectors beyond ④ and ⑤, including science/education/culture/health/sports and public administration	Similar to sector⑤	Yes	Science/education/culture/health/sports buildings	
⑦	Urban Residential Consumption	Urban household energy use	Primarily building energy use	Yes	Urban residential buildings	
⑧	Rural Residential Consumption	Rural household energy use	Primarily building energy use	Yes	Rural residential buildings	

Aside from the residential consumption categories ⑦ and ⑧, sectors ②, ④, ⑤, and ⑥ in the energy balance table also contribute to energy use in buildings. However, these sectors include the consumption of diesel and gasoline, which are primarily used for private enterprise or personal transportation and should be excluded.

In this study, residential consumption categories ⑦ and ⑧ in the energy balance table are assigned to the operational energy use of urban and rural residential buildings, respectively. Sector ⑤ (wholesale, retail, hotel, and catering) is attributed to the operational energy consumption of wholesale/retail/hotel/catering buildings, while sector ⑥ corresponds to science/education/culture/health/sports buildings. A portion of the energy consumed in sector ④—specifically that used in functional buildings such as stations, airports, and post offices—is allocated to transportation/warehouse/postal buildings. Following the approach of Wang et al. (2023), all coal consumption and 40% of electricity use in sector ④ are attributed to the operational energy use of public buildings, thereby excluding energy associated with private and public transportation. The industrial sector (sector ②) in the energy balance table represents energy consumption in secondary industries, including mining, manufacturing, and public utility production and supply. After excluding the mining component, the remaining energy use is attributed to emissions from industrial buildings.

Thus, the energy consumption $\mathrm{EC}^{c}_{\mathrm{building,i}}$ for building operations in city c can be expressed as:

$$\mathrm{EC}^{c}_{\mathrm{building,i}} = \mathrm{EC}^{c}_{\mathrm{Industrial,i}} + \mathrm{EC}^{c}_{\mathrm{Transport,i}} + \mathrm{EC}^{c}_{\mathrm{Wholesale,i}} + \mathrm{EC}^{c}_{\mathrm{Public,i}} + \mathrm{EC}^{c}_{\mathrm{Household,i}} \quad (3)$$

where I denotes each of the 20 energy types. $\mathrm{EC}^{c}_{\mathrm{Industrial,i}}$, $\mathrm{EC}^{c}_{\mathrm{Transport,i}}$, $\mathrm{EC}^{c}_{\mathrm{Wholesale,i}}$, $\mathrm{EC}^{c}_{\mathrm{Public,i}}$ and $\mathrm{EC}^{c}_{\mathrm{Household,i}}$ represent the energy consumption of industrial buildings, transportation/warehouse/postal buildings, wholesale/retail/hotel/catering buildings, science/education/culture/health/sports buildings, and residential buildings, respectively. Note that $\mathrm{EC}^{c}_{\mathrm{Household,i}}$ includes both urban and rural residential building energy use.

4.1.2 Bottom-Up Approach for Estimating Operational Carbon Emissions

In constructing the bottom-up inventory of building operational energy use and associated carbon emissions, this study adopts methodologies consistent with our previous work (Chen et al., 2025), particularly in the development of building databases (Supplementary Fig. 1), energy demand estimation, and energy conversion modules. From the perspective of energy demand, in residential buildings, specific energy consumption and related CO_2 emissions arise from activities such as cooking, lighting, cooling, water heating, laundry, and the operation of household appliances. For wholesale, retail, hotel, and catering buildings, energy use and emissions are quantified across multiple end-use sectors, including catering services, commercial HVAC systems, lighting, and electrical equipment. In science, education, culture, health, and sports buildings, energy consumption is estimated for public HVAC systems, lighting, electrical equipment, and power facilities.

The final energy consumption of buildings under the bottom-up approach is calculated using the following formula:

$$EC_n = \sum_i \sum_j AL_{n,i,j} \times EI_{n,i,j} \quad (4)$$

Where, n denotes the building type, covering six categories, i represents end-use equipment (e.g., cooking stoves, lighting, refrigerators, and electrical appliances in residential buildings), j indicates the energy type (e.g., direct Scope 1 emissions from coal, natural gas, and liquefied petroleum gas; indirect Scope 2 emissions from purchased electricity and heat). AL is the activity level parameter for energy-demanding economic activities. For instance, in the transportation sector, this might be represented as passenger-kilometers; in this study, it is approximated by the gross floor area of each building (footprint area × number of floors). Meanwhile, EI is the annual energy intensity of each end-use equipment.

Energy consumption during building operation includes both direct Scope 1 energy use and indirect Scope 2 final energy use. The corresponding formula is:

$$EC_n = EC_{n,scope1} + EC_{n,scope2} \quad (5)$$

Where $EC_{n,scope1}$ denotes direct energy consumption (Scope 1) for building type n, and $EC_{n,scope2}$ represents indirect energy consumption (Scope 2).

Similarly, for Scope 1 and Scope 2 carbon emissions resulting from energy consumption, the following formula is applied:

$$CE_n = CE_{n,scope1} + CE_{n,scope2} \quad (6)$$

Where CE_{scope1} and CE_{scope2} signifies the Scope 1 and Scope 2 carbon emissions, respectively.

For carbon emission accounting, this study adopts the emission factor method provided in the IPCC (2006) Guidelines for National Greenhouse Gas Inventories to estimate carbon emissions during building operation. The formula is as follows:

$$\mathrm{CE} = \sum_{\mathrm{i}=1}^{\mathrm{n}} \mathrm{AD_i} \times \mathrm{EF_i} \quad (7)$$

Where CE represents the total carbon emissions from building operations in the city, $\mathrm{AD_I}$ denotes the total consumption of energy type i, and $\mathrm{EF_i}$ is the carbon emission factor for energy type i. In this study, energy-related carbon emissions can be expressed as:

$$CE_{n,scope1} = \sum_{\mathrm{i}=1}^{\mathrm{n}} \mathrm{EC^c_{building,i}} \times \mathrm{NCV_i} \times \mathrm{CC_i} \times \mathrm{O_i} \quad (8)$$

Here, $\mathrm{EC^c_{building,i}}$ refers to the consumption of energy type i in building operations in city c, while $\mathrm{NCV_i}$, $\mathrm{CC_i}$ and $\mathrm{O_i}$ represent the net calorific value (J/ton), carbon content (ton CO_2/J), and oxidation rate (%), respectively. Different energy types are associated with specific emission coefficients for calculating CO_2 emissions. Although both IPCC (2006) and China's NDRC (2013) provide default emission factors for fossil fuels, Liu et al.(xx) found that these recommended factors tend to overestimate actual values based on measurements from 602 coal samples across China's 100 largest mining areas. Therefore, this study utilizes emission factors derived from extensive surveys of coal mines.

Additionally, indirect emissions from electricity and heat consumption ($CE_{n,scope2}$) are calculated as follows:

$$CE_{n,scope2} = \mathrm{CE_{electricity}} + \mathrm{CE_{heat}} = \mathrm{EC^c_{building,electricity}} \times \mathrm{EF_e} + \mathrm{EC^c_{building,heat}} \times \mathrm{EF_h} \quad (9)$$

Here, $EC^{c}_{building,electricity}$ and $EC^{c}_{building,heat}$ denote the consumption of electricity and heat in building operations in city c, respectively. EF_e and EF_h are the corresponding provincial-level carbon emission factors for electricity and heat adopted in this study.

When characterizing the supply side using point-source power plants to further disaggregate the energy structure of the power generation sector (Supplementary Fig.2), $CE_{n,scope2}$ can also be expressed in the following form:

$$CE_{n,scope2} = \sum_{s}\sum_{m}\sum_{t} ETP_{m,t} \times \frac{1}{f_{s,m,t}} \times EF_{s,m,t} \quad (10)$$

Where s designates the type of primary energy; m captures equipment attributes, including in this study power plant characteristics such as installed capacity, service lifetime, power generation technology, efficiency, and dispatch rules; and t indicates the type of secondary energy. The term $EF_{n,i,j}$ refers to the emission factor for energy type j consumed by end-use equipment i in building type n. On the other hand, $ETP_{m,t}$ denotes the amount of secondary energy type t ultimately consumed within the study boundary; $EF_{s,m,t}$ is the emission factor of point source unit m utilizing primary energy s to produce secondary energy t; and f stands for the conversion efficiency, expressed as a percentage.

4.1.3 A Coupled Top-Down and Bottom-Up Approach

Integrating macro-scale economic representation with micro-scale technological detail remains a central challenge in energy and emission modeling. To address this, we develop a coupled modeling framework that systematically embeds a technologically detailed bottom-up (BU) energy model within a macro-economically consistent top-down (TD) structure. This hybrid framework preserves engineering realism while ensuring consistency with national economic and energy accounts. Within this structure, outputs from the TD model provide aggregate constraints for the BU model, allowing for mutual calibration, validation, and iterative adjustment between the two modules. The resulting framework produces a coherent, multi-scale energy dataset that captures both disaggregated end-use energy characteristics and alignment with macro-level statistical energy balances. This reconciled dataset enhances the precision and contextual validity of operational carbon emission estimations. The mathematical formulations are presented as follows:

Let $E^{TD} \in R^{m}$ denote the vector of macro-level energy consumption by fuel type derived from the top-down model (e.g., based on national energy statistics or input-output analysis), and $E^{BU} \in R^{n}$ the vector of disaggregated energy use by end-use sectors and building types obtained from the bottom-up engineering model.

The coupling and reconciliation process is formulated as a constrained optimization problem:

$$Minimize \left|\left|W \cdot (E^{BU} - T \cdot E^{TD})\right|\right|^{2} \quad (11)$$

subject to:

$$A \cdot E^{BU} \leq b, \qquad E^{BU} \geq 0 \quad (12)$$

Where $T \in R^{n \times m}$ is a transformation matrix that maps macro-level energy vectors to disaggregated sectors, while W is a diagonal weighting matrix representing confidence levels or uncertainties in bottom-up data. Additionally, A and b define linear constraints representing technological and structural limits.

The reconciled energy consumption vector E^* is obtained by solving the above problem. This vector is then used to compute the total operational carbon emissions:

$$CE = \sum_j \left(E_j^* \cdot EF_j\right) \tag{13}$$

where EF_j is the emission factor for energy type j.

4.2 Metrics for Measuring Urban Form and Building Morphological Characteristics

4.2.1 Urban Form Metrics

Building Density. After delineating the urban boundary, the building density within the urban patch is calculated. Building density, defined as the ratio of the total building footprint area to the total built-up area, reflects the proportion of open space and the concentration of structures within the city. It is expressed as:

$$D = \frac{AREA_f}{AREA_b} \tag{14}$$

Where, D denotes the building density(dimensionless), $AREA_f$ is the total building footprint area (in consistent areal units, e.g., km²), and $AREA_b$ is the total built-up area within the urban boundary (in the same units).

Development Intensity. In this study, development intensity refers to the Floor Area Ratio (FAR), a key urban planning metric defined as the ratio of the total building floor area to the built-up area. This indicator effectively measures the intensity of land use within the urban boundary. The formula is given by:

$$I = \frac{I_a}{I_b} \tag{15}$$

Where, I represents the development intensity(dimensionless), I_a is the total building floor area, while I_b is the total built-up area. For calculations at administrative district and street levels, the built-up area data are sourced from the global urban boundary dataset published by Li et al. (2020)[61].

4.2.2 Building Morphological Metrics

Based on individual building data, this study computes multi-scale morphological features—average building height $\overline{H}$, average footprint area $\overline{A_f}$, and average floor area $\overline{A_t}$—at the city, district, and street levels. These are defined as follows:

- The **average building height** $\overline{H}$ is calculated as the footprint-area-weighted mean height of all buildings:

$$\overline{H} = \frac{\sum_{i=1}^{n}(AREA_i \times Hight_i)}{\sum_{i=1}^{n} AREA_i} \tag{16}$$

- The **average footprint area** $\overline{A_f}$ is computed as the height-weighted mean footprint area:

$$\overline{A_f} = \frac{\sum_{i=1}^{n}(AREA_i \times Hight_i)}{\sum_{i=1}^{n} Height_i} \tag{17}$$

- The **average floor area** $\overline{A_t}$ represents the arithmetic mean floor area per building:

$$\overline{A_t} = \frac{\sum_{i=1}^{n}(AREA_i \times Floor_i)}{n} \tag{18}$$

In these expressions, n denotes the total number of buildings, i indexes individual buildings, $AREA_i$ represents the footprint area of the i-th building, $Hight_i$ represents its height, and $Floor_i$ indicates its number of floors. Together, these metrics offer multi-scale insights into urban

morphological characteristics, facilitating further analysis of urban form and its functional implications.

5. Data Availability

The data generated in this study are provided in the Cloud Repository (https://cloud.tsinghua.edu.cn/d/d0c13192786a432d80e1/). Building data supporting the findings of this manuscript are also available from the corresponding author upon request.

6. Reference

1. Calvin, K. *et al. IPCC, 2023: Climate Change 2023: Synthesis Report. Contribution of Working Groups I, II and III to the Sixth Assessment Report of the Intergovernmental Panel on Climate Change [Core Writing Team, H. Lee and J. Romero (Eds.)]. IPCC, Geneva, Switzerland.* https://www.ipcc.ch/report/ar6/syr/ (2023) doi:10.59327/IPCC/AR6-9789291691647.
2. Li, S. *et al.* Revisiting Copenhagen climate mitigation targets. *Nat. Clim. Chang.* **14**, 468–475 (2024).
3. Iyer, G. *et al.* Ratcheting of climate pledges needed to limit peak global warming. *Nat. Clim. Chang.* **12**, 1129–1135 (2022).
4. United Nations Environment Programme *et al. Emissions Gap Report 2024: No More Hot Air … Please! With a Massive Gap between Rhetoric and Reality, Countries Draft New Climate Commitments*. (United Nations Environment Programme, 2024). doi:10.59117/20.500.11822/46404.
5. Liu, Z. *et al.* Challenges and opportunities for carbon neutrality in China. *Nat Rev Earth Environ* **3**, 141–155 (2021).
6. Global Times. Xi announces China's 2035 NDC to beef up climate response.

https://www.globaltimes.cn/page/202509/1344510.shtml.

7. IEA. *Empowering Urban Energy Transitions*. (2024).
8. UN-Habitat. *World Cities Report 2024*. (P.O. Box 30030, Nairobi, Kenya, 2024).
9. IEA. *Tracking Clean Energy Progress 2023*. https://www.iea.org/reports/tracking-clean-energy-progress-2023 (2023).
10. IEA. Global CO2 emissions from the operation of buildings in the Net Zero Scenario, 2010-2030. (2023).
11. Building Energy Research Center of Tsinghua University. *Decarbonize Urban Heating System: China Building Energy and Emission Yearbook 2023*. (Springer Nature Singapore, Singapore, 2024). doi:10.1007/978-981-99-7875-5.
12. Ma, M., Zhou, N., Feng, W. & Yan, J. Challenges and opportunities in the global net-zero building sector. *Cell Reports Sustainability* **1**, 100154 (2024).
13. Fenner, A. E. *et al.* The carbon footprint of buildings: A review of methodologies and applications. *Renewable and Sustainable Energy Reviews* **94**, 1142–1152 (2018).
14. Röck, M. *et al.* Embodied GHG emissions of buildings – The hidden challenge for effective climate change mitigation. *Applied Energy* **258**, 114107 (2020).
15. Yu, Y. *et al.* A city-level assessment framework for low-carbon transition of residential district heating in China. *Resources, Conservation and Recycling* **225**, 108576 (2026).
16. Deng, Y. *et al.* Provincial allocation of China's commercial building operational carbon toward carbon neutrality. *Applied Energy* **384**, 125450 (2025).
17. Zhang, S. *et al.* Historical carbon abatement in the commercial building operation:

China versus the US. *Energy Economics* **105**, 105712 (2022).

18. Hu, S. *et al.* Ecological Pathway to Achieve Carbon Neutrality in China's Building Sector. *Engineering* S2095809925003686 (2025) doi:10.1016/j.eng.2025.07.006.

19. Van Heerden, R. *et al.* Demand-side strategies enable rapid and deep cuts in buildings and transport emissions to 2050. *Nat Energy* **10**, 380–394 (2025).

20. Camarasa, C. *et al.* A global comparison of building decarbonization scenarios by 2050 towards 1.5–2 °C targets. *Nat Commun* **13**, 3077 (2022).

21. Rayegan, S. *et al.* Achieving carbon neutrality at single and multi-building complex levels – A review. *Energy and Buildings* **314**, 114263 (2024).

22. Chen, Y. *et al.* A building-scale modeling framework for urban net-zero transitions in Nanjing. *Nat Commun* **16**, 8954 (2025).

23. Xia, B. *et al.* Exploiting vacant urban residential buildings to promote carbon neutrality in China. *Nat Commun* **16**, 7661 (2025).

24. Güneralp, B. *et al.* Global scenarios of urban density and its impacts on building energy use through 2050. *Proc. Natl. Acad. Sci. U.S.A.* **114**, 8945–8950 (2017).

25. Tang, Y. *et al.* High resolution spatial distribution of CO_2 emissions from building operations and driving factors in the Guangdong-Hong Kong-Macao Greater Bay Area. *Sustainable Cities and Society* **131**, 106708 (2025).

26. Wang, J. *et al.* High-resolution temporal and spatial evolution of carbon emissions from building operations in Beijing. *Journal of Cleaner Production* **376**, 134272 (2022).

27. Creutzig, F., Baiocchi, G., Bierkandt, R., Pichler, P.-P. & Seto, K. C. Global

typology of urban energy use and potentials for an urbanization mitigation wedge. *Proc. Natl. Acad. Sci. U.S.A.* **112**, 6283–6288 (2015).

28. Boccalatte, A., Fossa, M., Gaillard, L. & Menezo, C. Microclimate and urban morphology effects on building energy demand in different European cities. *Energy and Buildings* **224**, 110129 (2020).

29. Arvidsson, M., Lovsjö, N. & Keuschnigg, M. Urban scaling laws arise from within-city inequalities. *Nat Hum Behav* **7**, 365–374 (2023).

30. Berghauser Pont, M. *Spacematrix: Space, Density and Urban Form - revised edition*. (TU Delft OPEN Publishing, Erscheinungsort nicht ermittelbar, 2023).

31. Cheshmehzangi, A. & Dawodu, A. Towards a Sustainable Energy Planning Strategy: The Utilisation of Floor Area Ratio for Residential Community Planning and Design in China. *Front. Sustain. Cities* **3**, 687895 (2021).

32. Javanroodi, K., Mahdavinejad, M. & Nik, V. M. Impacts of urban morphology on reducing cooling load and increasing ventilation potential in hot-arid climate. *Applied Energy* **231**, 714–746 (2018).

33. Dawodu, A. & Cheshmehzangi, A. Impact of Floor Area Ratio (FAR) on Energy Consumption at Meso Scale in China: Case Study of Ningbo. *Energy Procedia* **105**, 3449–3455 (2017).

34. Song, C. *et al.* Developing urban building energy models for shanghai city with multi-source open data. *Sustainable Cities and Society* **106**, 105425 (2024).

35. Milojevic-Dupont, N. *et al.* EUBUCCO v0.1: European building stock characteristics in a common and open database for 200+ million individual buildings.

Sci Data **10**, 147 (2023).

36. Yap, W., Wu, A. N., Miller, C. & Biljecki, F. Revealing building operating carbon dynamics for multiple cities. *Nat Sustain* https://doi.org/10.1038/s41893-025-01615-8 (2025) doi:10.1038/s41893-025-01615-8.

37. Yu, Y. *et al.* City-level building operation and end-use carbon emissions dataset from China for 2015–2020. *Sci Data* **11**, 138 (2024).

38. Jin, X. *et al.* Mitigating building carbon emissions in high-density cities considering energy sufficiency. *Applied Energy* **400**, 126586 (2025).

39. You, K. *et al.* Mitigating emissions and costs through demand-side solutions in Chinese residential buildings. *Nat Commun* **16**, 7358 (2025).

40. Naeem, A. *et al.* EnergyPlus as a computational engine for commercial building operational digital twins. *Energy and Buildings* **329**, 115257 (2025).

41. Haddad, S. *et al.* Quantifying the energy impact of heat mitigation technologies at the urban scale. *Nat Cities* **1**, 62–72 (2024).

42. Chen, Y., Hong, T. & Piette, M. A. Automatic generation and simulation of urban building energy models based on city datasets for city-scale building retrofit analysis. *Applied Energy* **205**, 323–335 (2017).

43. Weiler, V. *et al.* Automatic dimensioning of energy system components for building cluster simulation. *Applied Energy* **313**, 118651 (2022).

44. Yan, D. *et al.* DeST 3.0: A new-generation building performance simulation platform. *Build. Simul.* **15**, 1849–1868 (2022).

45. Wang, X., Tan, Y., Zhou, G., Jing, G. & John Francis, E. A framework for

analyzing energy consumption in urban built-up areas based on single photonic radar and spatial big data. *Energy* **290**, 130202 (2024).

46. Zhang, Y., Teoh, B. K., Wu, M., Chen, J. & Zhang, L. Data-driven estimation of building energy consumption and GHG emissions using explainable artificial intelligence. *Energy* **262**, 125468 (2023).

47. Ma, M., Ma, X., Cai, W. & Cai, W. Low carbon roadmap of residential building sector in China: Historical mitigation and prospective peak. *Applied Energy* **273**, 115247 (2020).

48. Berrill, P., Gillingham, K. T. & Hertwich, E. G. Linking Housing Policy, Housing Typology, and Residential Energy Demand in the United States. *Environ. Sci. Technol.* **55**, 2224–2233 (2021).

49. Krapf, S., Mayer, K. & Fischer, M. Points for energy renovation (PointER): A point cloud dataset of a million buildings linked to energy features. *Sci Data* **10**, 639 (2023).

50. Prieto-Curiel, R., Patino, J. E. & Anderson, B. Scaling of the morphology of African cities. *Proc. Natl. Acad. Sci. U.S.A.* **120**, e2214254120 (2023).

51. Huo, J., Meng, J., Zheng, H., Parikh, P. & Guan, D. Achieving decent living standards in emerging economies challenges national mitigation goals for CO2 emissions. *Nat Commun* **14**, 6342 (2023).

52. Hu, S., Jiang, Y. & Yan, D. *China Building Energy Use and Carbon Emission Yearbook 2021: A Roadmap to Carbon Neutrality by 2060*. (Springer Nature Singapore, Singapore, 2022). doi:10.1007/978-981-16-7578-2.

53. McKinnon, K. A., Simpson, I. R. & Williams, A. P. The pace of change of summertime temperature extremes. *Proc. Natl. Acad. Sci. U.S.A.* **121**, e2406143121 (2024).

54. Wan, K. K. W., Li, D. H. W., Pan, W. & Lam, J. C. Impact of climate change on building energy use in different climate zones and mitigation and adaptation implications. *Applied Energy* **97**, 274–282 (2012).

55. Yang, Y., Østergaard, P. A., Wen, W. & Zhou, P. Heating transition in the hot summer and cold winter zone of China: District heating or individual heating? *Energy* **290**, 130283 (2024).

56. Tang, H. *et al.* Assessment of BIPV power generation potential at the city scale based on local climate zones: Combining physical simulation, machine learning and 3D building models. *Renewable Energy* **244**, 122688 (2025).

57. Virtuani, A., Borja Block, A., Wyrsch, N. & Ballif, C. The carbon intensity of integrated photovoltaics. *Joule* **7**, 2511–2536 (2023).

58. CEADs. Carbon Emission Accounts and Datasets.

59. Yang, G. *et al.* A comprehensive city-level final energy consumption dataset including renewable energy for China, 2005–2021. *Sci Data* **11**, 738 (2024).

60. Shan, Y., Liu, J., Liu, Z., Shao, S. & Guan, D. An emissions-socioeconomic inventory of Chinese cities. *Sci Data* **6**, 190027 (2019).

61. Li, X. *et al.* Mapping global urban boundaries from the global artificial impervious area (GAIA) data. *Environ. Res. Lett.* **15**, 094044 (2020).

62. NEA. The construction and operation status of solar PV in 2021. (2022).

63. Shi, M., Lu, X. & Craig, M. T. Unveiling deployable rooftop solar potential across Chinese cities. *Nat Cities* **2**, 650–661 (2025).

7. Author Contributions Statement

Y.X.C. collected data, developed methodology, built models, performed formal analysis, created visualizations, and wrote the manuscript. K.P.R. contributed to data analysis and manuscript writing. Y.D.S. contributed to research design and data provision. Q.W. contributed to research design and methodology validation. D.L.L. performed data analysis and contributed to writing—review and editing. Y.L.S. provided supplementary data and materials. D.B.G. acquired funding, designed the research, supervised the project, and contributed to writing—review and editing.

8. Competing Interests Statement

The authors declare no competing interests.

Supplementary Files

This is a list of supplementary files associated with this preprint. Click to download.

- SupplementaryInformation.docx